Intrinsic excitability differs between murine hypoglossal and spinal motoneurons

MA Tadros[1], AJ Fuglevand[2], AM Brichta[1] and RJ Callister[1]

[1]School of Biomedical Sciences & Pharmacy, Faculty of Health and Hunter Medical Research Institute, The University of Newcastle, Callaghan, NSW 2308, Australia

[2]Department of Physiology, College of Medicine, University of Arizona, Tucson, AZ 85724, USA

Running Title: hypoglossal vs. spinal motoneurons

Key Words: motoneuron, excitability, action potential,

Address for correspondence:
Dr. R.J. Callister
School of Biomedical Sciences & Pharmacy
The University of Newcastle
Callaghan, NSW 2308
Australia
Phone: Int-61-2-4921-7808
Fax:Int-61-2-4921-8712
Email: robert.callister@newcastle.edu.au

Abstract

Motoneurons differ in the behaviours they control and their vulnerability to disease and ageing. For example, brainstem motoneurons such as hypoglossal motoneurons (HMs) are involved in licking, suckling, swallowing, respiration, and vocalization. In contrast spinal motoneurons (SMs) innervating the limbs are involved in postural and locomotor tasks requiring higher loads and lower movement velocities. Surprisingly, the properties of these two motoneuron pools have not been directly compared even though studies on HMs predominate in the literature compared to SMs, especially for adult animals. Here, we used whole cell patch clamp recording to compare the electrophysiological properties of HMs and SMs in age-matched neonatal mice (P7-10). Passive membrane properties were remarkably similar in HMs and SMs and afterhyperpolarization properties did not differ markedly between the two populations. HMs had narrower action potentials (AP), and a faster upstroke on their APs compared to SMs. Furthermore, HMs discharged APs at higher frequencies in response to both step and ramp current injection than SMs. Therefore, while HMs and SMs have similar passive properties, they differ in their response to similar levels of depolarizing current. This suggests each population possess differing suites of ion channels that allow them to discharge at rates matched to the different mechanical properties of the muscle fibers that drive their distinct motor functions.

Introduction

Motoneurons innervate striated muscle and ultimately drive movement, however, it has been recognized that motoneurons can differ considerably in their properties according to their target muscle (for reviews see: Kanning et al. 2010; Manuel and Zytnicki 2011). This is particularly the case for brainstem and spinal motoneurons. For example, brainstem hypoglossal motoneurons (HMs) innervate tongue musculature and are recruited in diverse motor functions such as swallowing, suckling, licking, and vocalization (Fregosi and Ludlow 2014). In addition, their activity must be synchronised with that of respiratory circuits (Feldman and Kam 2015) and thereby are engaged continuously throughout the lifespan of an animal. Furthermore, because the tongue has only one bony attachment, tongue muscles typically operate under relatively small load conditions. Spinal motoneurons (SMs), on the other hand, are primarily involved in postural, locomotor, and manipulation tasks that involve comparatively higher loads and lower velocity movements (Stifani 2014). At birth, HMs contribute to feeding and respiratory networks and subsequently undergo minor changes during the postnatal period (Greer and Funk 2005). In contrast, the postural and locomotor circuits involving SMs are immature at birth and subsequently take on adult properties over the first two postnatal weeks in rodents (Vinay et al. 2000). Despite these functional and developmental differences, the intrinsic and cellular properties of these two motoneuron populations are poorly understood.

It has also been known for some time that ageing, disease, and injury affect HMs and SMs in different ways. For example, in the rat, ageing leads to a significant decrease in SM numbers with no concomitant loss of HMs (Ishihara et al. 1987; Schwarz et al. 2009). Similarly, rat hindlimb muscle force is reduced markedly several months before deficits of tongue musculature are observed during ageing (Horner et al. 2011; Ota et al. 2005). In contrast, patients with certain motoneuron diseases (such as amyotrophic lateral sclerosis; ALS) often present with speaking difficulties well before locomotor defects are observed (Langmore and Lehman 1994). Brainstem and spinal motoneurons also exhibit distinctly different responses to peripheral nerve injury, with greater re-expression of the growth factor p75 and attenuated downregulation of choline acetyltransferase (ChAT) immunoreactivity in HMs compared to SMs in response to axotomy (Rende et al. 1995). Together, these studies

81 suggest HMs and SMs have altered susceptibility to disease and emphasize the need
82 to understand more about the underlying cellular properties of these two neuronal
83 populations.
84
85 Despite differences in function and disease susceptibility, studies on the neural control
86 of movement often fail to separate motoneurons into distinct categories (Manuel and
87 Zytnicki 2011). Whilst elegant studies have used mice and sophisticated molecular
88 and transgenic techniques to investigate the development and connectivity of
89 motoneurons with premotor circuitry (Miles et al. 2004; Zagoraiou et al. 2009), there
90 is a lack of comprehensive studies examining the intrinsic properties of motoneuron
91 populations in the wild type mouse. Therefore, the main purpose of this study was to
92 directly compare the electrophysiological properties of a representative population of
93 brainstem (i.e., hypoglossal) and spinal (i.e., lumbar) motoneurons in age matched
94 wild type mice to test the hypothesis that these two categories of motoneurons possess
95 distinct properties subserving their differing functions.
96

Methods

Tissue Preparation

All procedures were approved by the University of Newcastle Animal Care and Ethics Committee. Neonatal mice (C57Bl/6, both sexes, P7 – P10) were anaesthetised with ketamine (100 mg/kg i.p.) and decapitated. The brainstem or lumbosacral enlargement of the spinal cord was rapidly removed to obtain slices containing the hypoglossal nucleus or lumbar spinal motoneurons. The tissue was immediately immersed in ice-cold sucrose-substituted artificial cerebrospinal fluid (sACSF) containing (in mM): 250 sucrose, 25 $NaHCO_2$, 10 glucose, 2.5 KCl, 1 NaH_2PO_4, 1 $MgCl_2$ and 2.5 $CaCl_2$, continuously bubbled with 95% O_2 and 5% CO_2 to achieve pH of 7.3. Transverse slices (300 μm thick) were obtained from the brainstem region containing the hypoglossal nucleus (~ 0.5 mm above and below the obex) and from L3-5 spinal cord segments using a vibrating-blade microtome (Leica VT1200s, Leica Microsystems, Wetzlar, Germany). Three to four consecutive slices from the brainstem or spinal cord were transferred to a humidified storage chamber containing oxygenated ACSF (118 mM NaCl substituted for sucrose in sACSF). Slices were allowed to recover for 1 hour at room temperature (22-24^{o}C) prior to recording.

Electrophysiology

Slices were transferred to a recording chamber, and held in place using nylon netting fixed to a U-shaped platinum frame. The recording chamber was continually perfused with oxygenated ACSF (4-6 bath volumes/minute) and maintained at a constant temperature (23^{o}C) via an in-line temperature control device (TC-324B, Warner Instruments, Hamden, CT). Whole cell patch clamp recordings were made from visualized motoneurons using infrared differential contrast optics (IR-DIC optics) and an IR-sensitive camera (Rolera-XR, Olympus, NJ). Recordings were obtained from hypoglossal motoneurons (HMs) in brainstem slices, and lumbar motoneurons (SMs) in spinal cord slices. Motoneurons were identified according to the following criteria: their large soma size (diameter 20-35 μm vs. 10-15 μm for local interneurons), high capacitance (> 35 pF), low input resistance and ability to produce tonic AP discharge (Carlin et al. 2000a; Carlin et al. 2000b; Tadros et al. 2014).

Intrinsic properties of MNs

Patch pipettes (3-4 MΩ resistance) were prepared from thin walled borosilicate glass (PG150T-15, Harvard Apparatus, Kent, UK), and filled with a potassium-based

internal solution containing (in mM): 135 KCH_3SO_4, 6 NaCl, 2 $MgCl_2$, 10 HEPES, 0.1 EGTA, 2 MgATP, 0.3 NaGTP, pH 7.3 (with KOH). Whole cell patch clamp recordings were made using a Multiclamp 700B Amplifier (Molecular Devices, Sunnyvale, CA). The whole cell recording configuration was first established in voltage clamp mode (holding potential -60 mV). Series resistance was measured from the averaged response (five trials) to a 5 mV hyperpolarising pulse. This was assessed at the beginning and end of each recording session and data were rejected if values changed by > 20%. Input resistance was then calculated in current clamp across a minimum of four voltage responses to incrementally increasing hyperpolarising current injections (50 pA increments). In addition to the above measures, spontaneous excitatory postsynaptic currents (sEPSCs) were also recorded in voltage clamp for 60-120 s from a holding potential of -70 mV.

Several stimulus protocols were then applied to each motoneuron to study its intrinsic properties. We assessed the properties of the afterhyperpolarization (AHP) current by delivering a 2 ms pulse to depolarise the cell from a holding potential of -60 mV to -10 mV. The recording mode was then switched to current clamp, and the membrane potential ~ 15 s later was taken as resting membrane potential (RMP). All membrane potential values have been corrected for a calculated -10 mV liquid junction potential (Barry and Lynch 1991). To record single APs in current clamp, a series of short duration depolarising steps (20 pA increments, 2 ms duration) were applied from RMP. Small bias currents (< 50 pA) were then injected into the recorded motoneuron to maintain membrane potential at -70 mV. Repetitive discharge properties were then examined from this potential by applying two current protocols: 1) a series of depolarizing and hyperpolarising current steps (50 pA increments, 1 s duration); and 2) a triangular ramp current (0.33 nA/s, 3.5 seconds, 1 nA peak current).

Data Capture and Analysis

Data were digitised on-line (sampled at 20 kHz, sEPSCs filtered at 2 kHz, all other data filtered at 6 kHz) via an ITC-16 computer interface (Instrutech, Long Island, NY) and stored on a Macintosh computer using Axograph X software (Molecular Devices, Sunnyvale, CA). All data were analysed offline using the Axograph software. sEPSCs were detected and captured using a scaled template method (Clements and Bekkers 1997; Graham et al. 2011). Upon inspection, events were rejected if they overlapped or did not include a stable baseline before the rising phase of the captured event.

Several sEPSC parameters were measured, including peak amplitude, rise and decay time. The AHP recorded in voltage clamp was averaged (10 trials) and the amplitude and latency of the maximum outward current after the large inward current (or action current) were measured (Callister et al. 1997). An exponential was fit to the decay phase of the response to calculate the AHP current decay time constant. The onset of individual APs were identified using the derivative-threshold method to detect the inflection point; with dV/dt threshold set at 20 mV/ms. AP properties were measured from rheobase APs, generated by short duration depolarising steps (20 pA increments, 2 ms duration). The rheobase current was taken as the minimum current step that would evoke one AP. The difference between the membrane potential at AP threshold and maximum positive peak was taken as AP amplitude. AP half-width was measured at 50% of the AP's maximum peak. AHP amplitude, recorded in current clamp, was measured as the difference between AP threshold and the minimum membrane potential. The attenuation ratio was calculated by dividing the amplitudes of the last by the first AP discharged across a single current step. Derivatives of rheobase APs were generated in Axograph and the peak velocity was measured as the peak of the first derivative. Peak voltage acceleration was measured on the second derivative and the voltage acceleration at the axon initial segment (AIS) was taken as the first peak of the second derivative, as described by Wimmer et al. 2010.

The derivate threshold method was also used to detect APs evoked during injection of depolarising steps and triangular current ramps. We calculated the instantaneous frequency as the reciprocal of the interspike interval. Mean AP frequency was calculated as the average of all instantaneous frequencies for APs evoked by a single current step. Frequency/current plots (F/I plots) were generated using mean frequency (per current step) and the corresponding current amplitude, normalised to rheobase for comparison. For APs discharged in response to triangular current injection, instantaneous AP frequency was calculated as above and the currents associated with onset (recruitment current) and cessation of spiking (de-recruitment current) were measured. The difference between these two values (ie, de-recruitment current minus recruitment current – abbreviated ΔI) was then calculated (Bennett et al. 2001). Frequency/time and F/I plots were generated in order to assess changes in frequency on the ascending and descending arms of the triangular ramp current. The ramp gain was calculated as the ratio of change in firing rate to change in injected current (Hz/pA) across the first 10 APs discharged on the ascending phase of the ramp.

202

203 ***Statistics***

204 To avoid the limitations of null-hypothesis testing, effect sizes (ES, or *Cohen's d*)
205 were calculated (Cumming 2014). The effect size statistic identifies the magnitude of
206 differences in means between categories, and can reveal important biologically
207 relevant effects without sacrificing statistical power (Rank et al. 2015). Therefore, we
208 calculated the *Cohen's d* for all variables measured in HMs and SMs, and used this
209 value to determine the magnitude of the difference between the means (i.e., the effect
210 size). We designated values of $d < 0.2$ to indicate a trivial effect size, d of 0.2 to 0.5 a
211 small effect size, d of 0.5 to 0.8 as a moderate effect and $d > 0.8$ to indicate a large
212 effect. G-tests, with Williams' correction, were used to determine if the incidence of
213 rebound spiking differed between AP discharge categories. All data are presented as
214 means ± SEM.

215 ***Results***

216

217 A total of 54 recordings were obtained from motoneurons located in either the
218 hypoglossal nucleus (HMs; n = 28) or lumbosacral spinal cord (SMs; n = 26) from
219 age-matched mice (~ 8 days old, Table 1). The recording conditions, as assessed by
220 series resistance and holding current, did not differ between HMs and SMs (data not
221 shown).

222

223 ***Membrane and action potential properties***

224

225 Results for membrane and action potential properties for HMs and SMs are shown in
226 Table 1. SMs tended to have a larger input resistance (R_{IN}; ES moderate, d = 0.6),
227 more depolarised RMP and lower rheobase current (ES moderate, d = 0.55 and 0.54,
228 respectively) compared to HMs. AP threshold was similar in HMs and SMs, as was
229 AP amplitude, although AHP amplitude was slightly larger in HMs (ES moderate, d =
230 0.57). HMs displayed faster AP rise times and a greater velocity on the upstroke of
231 the AP compared to SMs (ES large, d = 1.2 and 0.87, respectively). Furthermore,
232 comparison of the second derivative of the rheobase AP, which provides an
233 estimation of the voltage acceleration of the membrane during AP discharge, revealed
234 a greater initial voltage acceleration in HMs compared to SMs (ES large, d = 1.4).
235 This initial voltage acceleration represents the activation of voltage-gated sodium
236 (Na^+) channels at the axon initial segment (AIS), which subsequently drives the
237 generation of the somatic AP (Wimmer et al. 2010). AP half-width was also
238 significantly longer in SMs. Taken together, these findings indicate that SMs
239 discharge broader and slower APs compared to HMs, which could be suggestive of
240 relatively more mature, therefore faster, spiking conductances in HMs.

241

242 In addition to the above parameters measured in current clamp, the outward current
243 underlying the AHP was also recorded in voltage clamp mode (Figure 1). Although
244 the peak amplitude was larger in HMs (ES moderate, d = 0.55), the time to peak and
245 decay time constant of the underlying AHP current did not differ between HMs and
246 SMs (ES small, d = 0.24 and 0.26, respectively). Taken together, these results suggest
247 that HMs and SMs have slightly different intrinsic membrane properties, with subtle
248 differences in the amplitude of their AHPs and in the speed of their APs, which may
249 impact their repetitive firing.

Repetitive discharge

Injection of current steps of increasing amplitude (50 pA increments, 1 s duration, from a membrane potential of -70 mV) was used to evoke repetitive discharge in both HMs and SMs (Figure 2A). All recorded neurons discharged tonically during current injection and mean discharge frequency was proportional to the injected current (Figure 2B). Mean frequency was calculated for each current step in order to examine the steady-state *F/I* relationship for the recorded neuron. To facilitate comparisons between HMs and SMs, current values were normalised to the rheobase current observed during 1 second step current injection of each neuron, and the *F/I* plot displayed in Figure 2B shows the relationship between discharge frequency and current (in pA) above rheobase. To examine the excitability of HMs and SMs, we compared the minimal frequency of AP discharge observed at rheobase for each population. HMs discharged APs at higher mean frequencies compared to SMs at rheobase and the next two successive current intensities (Figure 2B, Table 1). In addition, higher discharge frequencies were also observed in HMs compared to SMs at the highest current intensity examined (400 pA above rheobase). Furthermore, at these higher current intensities, HMs continued to discharge with consistent inter-event intervals, whereas SM firing became more variable. Of course this observation may be due to the greater heterogeneity in SMs compared to HMs.

We compared the slope, or gain, of the *F/I* relationship across the first 6 successive current intensities as these amplitudes resulted in the most consistent AP discharge in both populations. No difference in F/I gain was observed between HMs and SMs (F/I gain: 0.068 ± 0.004 vs. 0.075 ± 0.008 Hz/pA; R^2 values: 0.969 ± 0.007 vs. 0.954 ± 0.009), despite the aforementioned differences in mean firing frequency (Table 1). Maximal firing frequency was not measured, as we did not deliver sufficient current to cause depolarization blockade of APs (e.g. Pilarski et al. 2011).

Since differences in firing frequency have been attributed to altered Na^+ channel inactivation (Powers and Binder 2001), we next compared the initial AP amplitude of each successive current step between HMs and SMs as a relative measure of Na^+ inactivation. Although AP amplitude decreased as current intensity increased, we found no differences in the amplitude of the initial AP between HMs and SMs at any

current intensity (Rheobase: 60.17 ± 2.17 vs. 65.97 ± 2.78 mV, d = 0.45, ES small; 400 pA above rheobase: 55.02 ± 2.02 vs. 49.53 ± 2.86 mV, d = 0.43, ES small). In order to compare the Na^+ inactivation across a current step, we also compared the attenuation ratio (ie, relative amplitudes of the last and first AP) of each current step. Similarly, we found an increase in the attenuation of AP amplitude as current intensity increased, but again this was not different between HMs and SMs (Rheobase: 0.98 ± 0.02 vs. 1.01 ± 0.73 mV, d = 0.12, ES trivial; 400 pA above rheobase: 0.72 ± 0.03 vs. 0.66 ± 0.05 mV, d = 0.31, ES small). Taken together, this suggests Na^+ inactivation is similar during depolarization for the two populations of motoneurons.

In addition to applying current steps, we also injected triangular ramp currents (0.33 nA/s, holding potential -70 mV). Current ramps were used as an alternative way to evaluate the relation between depolarizing current and spike frequency and are also used to test for the presence of persistent inward currents in motoneurons (Bennett et al. 2004; ElBasiouny et al. 2010; Tadros et al. 2014). Figure 3A shows the response of a representative HM to triangular ramp current injection, with the onset and cessation of AP discharge indicated (*on* and *off*, respectively). Similar to step currents, we observed significantly higher *peak* discharge frequencies in HMs compared to SMs (ES large, d = 1.2; Figure 3B). It must be noted, however, that this was the peak discharge frequency observed for each MN in response to a single triangular ramp (0.33 nA/s, 1 nA peak current), and not the *maximal* frequency before AP discharge was abolished. Frequency/time (Figure 3C) and F/I (Figure 3D) plots were also generated for each motoneuron to assess changes in firing frequency during triangular ramp injection. This revealed relatively stable rates of increase in firing frequency during the ascending phase, and decrease in firing frequency during the descending phase for all motoneurons in both populations. As outlined in the *Methods*, ΔI was calculated for each neuron to provide an indirect assessment of the influence of two competing active conductances: one relating to spike-frequency adaptation (resulting in positive ΔI values) and one associated with persistent inward currents (PICs; resulting in negative ΔI values). Histograms of ΔI values were constructed for HMs (Figure 3E) and SMs (Figure 3F) so the distributions could be compared in the two populations. Mean ΔI values did not differ between HMs and SMs (HMs: +2.51 ± 2.4 vs. SMs: -0.60 ± 2.4; Table 1; ES small, d = 0.3). Furthermore, mean ΔI value for HMs and SMs were very small (less than 1% of rheobase current) and neither were

significantly different from 0.0 (single sample t-tests, HMs: $p = 0.32$; SMs, $p = 0.80$). This observation is in stark contrast to the substantial PICs (~ 50% of rheobase) observed, for example, in adult sacral MNs of rats following spinal cord injury (Bennett et al. 2001). To further assess the possible impact of any underlying PICs on AP discharge, we also compared the AP threshold and peak velocity of the first AP elicited in response to triangular ramp injection. Interestingly, although HMs displayed a more depolarized AP threshold during the triangular ramp injection compared to SMs (HMs: -32.0 ± 2.2 vs. SMs: -38.4 ± 2.9 mV; ES moderate, $d = 0.7$), the rate of rise was similar between the two populations. Taken together, the similarities in the velocity of the initial AP and ΔI values suggest any underlying PICs do not differ between HMs and SMs.

Reponses to hyperpolarization

We also compared the responses of HMs and SMs to hyperpolarizing current injections. Hyperpolarization of motoneurons in current clamp is often used to assess the presence and properties of the hyperpolarization-activated mixed cationic inward current (I_H). This current is thought to influence AP discharge frequency in adult HMs (Bayliss et al. 1994) and neonatal SMs (Takahashi 1990b). The responses of HMs and SMs to hyperpolarization were assessed by injection of hyperpolarizing current steps of increasing amplitude (-50 pA increments, 1 s duration) until peak membrane hyperpolarization reached about -110 mV (Figure 4A). The presence of I_H resulted in a depolarizing "sag" during the hyperpolarizing current step. This was quantified as the ratio between the membrane potential at the onset of hyperpolarization (Figure 4A, solid triangle) to the steady state membrane potential immediately prior to the release of the current step (Figure 4A, open triangle). Sag ratios (Figure 4B) did not differ between HMs and SMs (ES small, $d = 0.47$) and suggests that I_H expression is similar in each population of motoneurons. Following release from hyperpolarization, all motoneurons exhibited some degree of rebound depolarization. In a subset of both HMs and SMs, this rebound depolarization was sufficient to induce AP discharge (Figure 4A). Although slightly greater numbers of SMs displayed rebound AP discharge, the proportions of motoneurons with rebound AP discharge did not differ (G-test, with Williams' correction, $p = 0.19$; Figure 4C). Overall, these data suggest similar underlying cellular mechanisms in HMs and SMs drive responses to hyperpolarization.

Spontaneous excitatory synaptic currents

We recorded excitatory postsynaptic currents (sEPSCs; holding potential -70 mV) to assess residual spontaneous synaptic drive to HMs and SMs in brainstem and spinal cord slices (Figure 5). sEPSCs represent the postsynaptic response to neurotransmitter release from presynaptic terminals, and are observed as downward deflections on the current traces (Figure 5A). Mean sEPSC frequency was greater in SMs compared to HMs (ES moderate, d = 0.62; Figure 5C). sEPSC parameters were measured on averaged sEPSCs generated from all recorded sEPSCs for each neuron (Figure 5B). SMs had greater averaged sEPSC amplitudes (ES large, d = 0.89, Figure 5D) and faster rise (ES large, d = 0.89, Figure 5E) and decay times (ES moderate, d = 0.59, Figure 5F) compared to HMs. Taken together, this analysis suggests excitatory drive differs in SMs compared to HMs.

Discussion

This study presents a systematic comparison of the properties of age-matched brainstem and spinal motoneurons in neonatal wild type mice. Patch clamp studies of motoneurons have typically involved HMs because of their increased viability under in vitro conditions (i.e., slices), however, to our knowledge a direct comparison of HMs and SMs has never been conducted. We show that HMs and SMs have similar intrinsic properties, however, they differ in their intrinsic excitability with HMs being able to generate significantly higher discharge frequencies in response to both step and ramp current injection compared to SMs. Factors that might influence such differences in firing rate between SMs and HMs are discussed below.

Lower firing frequency in spinal motoneurons

A major finding of this study is the increased firing frequency observed in HMs compared to SMs during both step (Figure 2) and triangular ramp current injection (Figure 3). Several intrinsic membrane properties are known to contribute to firing rate (Bean 2007; Kernell 1999) and we compared many of these in the two motoneuron populations. In motoneurons, the primary factor determining the minimum firing frequency is the AHP duration (Kernell 1965). Although we did not specifically measure AHP duration in this study, we can infer that the AHP duration would be similar since we did not observe any differences in the AHP time course of HMs and SMs (Figure 1D). Although we did observe subtle differences in the amplitude of the AHP current, the similarities in AHP duration implies that additional factors are contributing to the decreased firing frequency we observed in SMs. Indeed, we observed shorter AP half-widths, faster AP velocity and greater voltage acceleration in HMs (Table 1). It is possible that the properties of sodium (Na^+) channels located at the axon initial segment (Kole and Stuart 2012) could explain these differences. For example, Na^+ current kinetics between HMs and SMs could contribute to the disparity in discharge frequencies we observed. However, Na^+ inactivation, as estimated by comparing AP threshold and attenuation ratio during current step injection, and PICs observed during triangular ramp injection were similar in the two populations. Thus, these two measures cannot fully explain the increased AP discharge frequency observed in HMs vs SMs.

Another potential contributor to motoneuron excitability is the non-specific, cationic current I_H (Biel et al. 2009). Whilst we did not investigate the properties of this current in voltage clamp, we were able to make inferences about its relative strength by measuring the "sag" during membrane hyperpolarization (Tadros et al. 2014; Figure 4). No differences were observed in the degree of sag between HMs and SMs, which is not surprising, given that anatomical studies have shown similar distributions of HCN channels, responsible for the I_H current, on HMs and SMs (Milligan et al. 2006). Furthermore, electrophysiological recordings have also shown similar reversal potentials and half-maximal activations of I_H in HMs (Bayliss et al. 1994) and SMs (Takahashi 1990a). In contrast, however, we did observe a higher proportion of SMs displaying rebound spiking (although not statistically significant), which can be linked either to the rebound from I_H, or T-type calcium currents elicited by depolarization (Rivera-Arconada and Lopez-Garcia 2015). Both HMs and SMs are known to express a number of calcium conductances, including the T-type calcium current during development (Mynlieff and Beam 1992; Umemiya and Berger 1994). However, to our knowledge, no data exist on the presence of calcium currents in either HMs or SMs at P8 so it is not known if these currents still play a role in generating the rebound spiking we observed in our sample.

Motoneuron diversity

Many studies have attempted to subdivide and classify motoneurons (for review see: Kanning et al. 2010). One such classification system is based on the contractile properties of the muscle fibres innervated by single motoneurons with slow-twitch fatigue-resistant (S) and fast-twitch fatigable (FF) fibres being at each end of a continuum. Using this classification, functional differences have been observed in the electrical properties of motoneurons innervating type S or FF fibres. In decerebrate cat preparations, type S motoneurons are more likely to display lower activation thresholds and are capable of sustained maximal firing rates for longer than type FF motoneurons (Lee and Heckman 1998). Additionally, a correlation between shorter, faster AHPs and type FF motoneurons has been observed in rats (Bakels and Kernell 1993; Gardiner 1993), which would result in faster firing frequencies in FF motoneurons. Interestingly, studies of muscle fibre types in the genioglossus, a major tongue protractor, has revealed a high proportion of FF fibres in the human (~ 70%; Yarom et al. 1986), cat (~ 75%; Hellstrand 1980) and rat (> 90%; Brozanski et al.

1993). This suggests the majority of HMs would innervate FF fibres and subsequently should display greater firing frequencies as observed in our HM sample. In contrast, SMs in the lumbosacral spinal cord would innervate a much wider range of muscle fibre types located in the highly variable muscles of the hindlimb, and thus include a more diverse motoneuron mix compared to the hypoglossal nucleus.

Motoneuron diversity exists across mammalian species. Historically cats were the preferred model for investigating motoneuron properties (for historical perspective see: Stuart and Brownstone 2011). Recently, motor control studies have included mice to take advantage of genetically modified murine models of human motoneuron disease (Brownstone and Stuart 2011). This transition from cat to mice has revealed several differences in the intrinsic, and cellular properties of motoneurons across species. Notably, in vivo intracellular recordings from mouse SMs have revealed greater discharge frequencies than those observed in cats or even rats. These high discharge frequencies are underpinned by a shorter membrane time constant and faster AHPs (Manuel et al. 2009). Similar comparisons between species do not exist for HMs, however, previous studies on developing HMs (aged P9) in rat have demonstrated firing frequencies of ~ 20 Hz in response to a 400 pA current injection (Viana et al. 1995). This is lower than the mean frequency we observed in mouse HMs at the highest current intensity applied (~ 30 Hz at 400 pA above rheobase, Figure 2B). In addition to these differences in firing rates, we did not observe any variability in acceleration of firing frequency during triangular ramp current injection as observed in previous studies in cat motoneurons (Lee and Heckman 1998). This could be due to methodological concerns (ie, in vitro vs. in vivo, whole-cell vs. intracellular recordings). Whilst there is no equivalent electrophysiological data on intrinsic and cellular properties of postnatal human motoneurons (but see Tadros et al. 2015 for data on fetal MNs), their discharge rates can be determined by recording the firing patterns of single motor units located in their target muscle. Interestingly, the relative difference in firing rates between HMs and SMs in the mouse (reported here) is also observed in adult human motor units. For example, the minimum rate of sustained discharge for human genioglossus motor units (innervated by HMs) is about 13 Hz (Bailey et al. 2007) whereas the minimum rate for typical limb-muscle motor units (innervated by SMs) is about 8 Hz (Milner-Brown et al. 1973; Monster and Chan 1977). Likewise, the saturation firing rate for low threshold genioglossus motor units in humans is ~ 24 Hz (Bailey et al. 2007) whereas it is ~ 15 Hz for biceps

474 brachii motor units (Fuglevand et al. 2015). Taken together, these studies provide
475 evidence that motoneuron firing rates vary between populations in a manner that fits
476 with their motor behaviour, and that this relative difference is conserved across
477 mammalian species.
478
479 ***Conclusions***
480
481 In this study, we have demonstrated significant differences in the intrinsic excitability
482 and excitatory drive between HMs and SMs of age-matched, wild-type mice. This
483 provides evidence that despite their common role as drivers of movement,
484 motoneuron populations can display differences in their properties that may arise
485 from subtle differences in their underlying ionic conductances and synaptic inputs.
486 These findings form a foundation for future studies elucidating the underlying
487 mechanisms resulting in altered susceptibility to disease and ageing between
488 motoneuron populations.
489
490

Acknowledgements: This work was supported by NIH grant #R01NS079147, and NH&MRC project grants (#s 401244, 569206, 628765, 631000) and the Hunter Medical Research Institute.

References

Bailey EF, Rice AD, and Fuglevand AJ. Firing patterns of human genioglossus motor units during voluntary tongue movement. *J Neurophysiol* 97: 933-936, 2007.

Bakels R, and Kernell D. Matching between motoneurone and muscle unit properties in rat medial gastrocnemius. *J Physiol* 463: 307-324, 1993.

Barry PH, and Lynch JW. Liquid junction potentials and small cell effects in patch-clamp analysis. *J Membr Biol* 121: 101-117, 1991.

Bayliss DA, Viana F, Bellingham MC, and Berger AJ. Characteristics and postnatal development of a hyperpolarization-activated inward current in rat hypoglossal motoneurons in vitro. *J Neurophysiol* 71: 119-128, 1994.

Bean BP. The action potential in mammalian central neurons. *Nat Rev Neurosci* 8: 451-465, 2007.

Bennett DJ, Li Y, and Siu M. Plateau potentials in sacrocaudal motoneurons of chronic spinal rats, recorded in vitro. *J Neurophysiol* 86: 1955-1971, 2001.

Bennett DJ, Sanelli L, Cooke CL, Harvey PJ, and Gorassini MA. Spastic long-lasting reflexes in the awake rat after sacral spinal cord injury. *J Neurophysiol* 91: 2247-2258, 2004.

Biel M, Wahl-Schott C, Michalakis S, and Zong X. Hyperpolarization-activated cation channels: from genes to function. *Physiol Rev* 89: 847-885, 2009.

Brownstone RM, and Stuart DG. Whither motoneurons? *Brain Res* 1409: 93-103, 2011.

Brozanski BS, Daood MJ, Watchko JF, LaFramboise WA, and Guthrie RD. Postnatal expression of myosin isoforms in the genioglossus and diaphragm muscles. *Pediatric pulmonology* 15: 212-219, 1993.

Callister RJ, Keast JR, and Sah P. Ca(2+)-activated K+ channels in rat otic ganglion cells: role of Ca2+ entry via Ca2+ channels and nicotinic receptors. *J Physiol* 500 (Pt 3): 571-582, 1997.

Carlin KP, Jiang Z, and Brownstone RM. Characterization of calcium currents in functionally mature mouse spinal motoneurons. *Eur J Neurosci* 12: 1624-1634, 2000a.

Carlin KP, Jones KE, Jiang Z, Jordan LM, and Brownstone RM. Dendritic L-type calcium currents in mouse spinal motoneurons: implications for bistability. *Eur J Neurosci* 12: 1635-1646, 2000b.

Clements JD, and Bekkers JM. Detection of spontaneous synaptic events with an optimally scaled template. *Biophys J* 73: 220-229, 1997.

Cumming G. The new statistics: why and how. *Psychol Sci* 25: 7-29, 2014.

ElBasiouny SM, Schuster JE, and Heckman CJ. Persistent inward currents in spinal motoneurons: important for normal function but potentially harmful after spinal cord injury and in amyotrophic lateral sclerosis. *Clin Neurophysiol* 121: 1669-1679, 2010.

Feldman JL, and Kam K. Facing the challenge of mammalian neural microcircuits: taking a few breaths may help. *J Physiol* 593: 3-23, 2015.

Fregosi RF, and Ludlow CL. Activation of upper airway muscles during breathing and swallowing. *J Appl Physiol (1985)* 116: 291-301, 2014.

Fuglevand AJ, Lester RA, and Johns RK. Distinguishing intrinsic from extrinsic factors underlying firing rate saturation in human motor units. *J Neurophysiol* 113: 1310-1322, 2015.

Gardiner PF. Physiological properties of motoneurons innervating different muscle unit types in rat gastrocnemius. *J Neurophysiol* 69: 1160-1170, 1993.

Graham BA, Tadros MA, Schofield PR, and Callister RJ. Probing glycine receptor stoichiometry in superficial dorsal horn neurones using the spasmodic mouse. *J Physiol* 589: 2459-2474, 2011.
Greer JJ, and Funk GD. Perinatal development of respiratory motoneurons. *Respir Physiol Neurobiol* 149: 43-61, 2005.
Hellstrand E. Morphological and histochemical properties of tongue muscles in cat. *Acta physiologica Scandinavica* 110: 187-198, 1980.
Horner AM, Russ DW, and Biknevicius AR. Effects of early-stage aging on locomotor dynamics and hindlimb muscle force production in the rat. *J Exp Biol* 214: 3588-3595, 2011.
Ishihara A, Naitoh H, and Katsuta S. Effects of ageing on the total number of muscle fibers and motoneurons of the tibialis anterior and soleus muscles in the rat. *Brain Res* 435: 355-358, 1987.
Kanning KC, Kaplan A, and Henderson CE. Motor neuron diversity in development and disease. *Annu Rev Neurosci* 33: 409-440, 2010.
Kernell D. The Limits of Firing Frequency in Cat Lumbosacral Motoneurones Possessing Different Time Course of Afterhyperpolarization. *Acta physiologica Scandinavica* 65: 87-100, 1965.
Kernell D. Repetitive impulse firing in motoneurons: facts and perspectives. *Prog Brain Res* 123: 31-37, 1999.
Kole MH, and Stuart GJ. Signal processing in the axon initial segment. *Neuron* 73: 235-247, 2012.
Langmore SE, and Lehman ME. Physiologic deficits in the orofacial system underlying dysarthria in amyotrophic lateral sclerosis. *J Speech Hear Res* 37: 28-37, 1994.
Lee RH, and Heckman CJ. Bistability in spinal motoneurons in vivo: systematic variations in rhythmic firing patterns. *J Neurophysiol* 80: 572-582, 1998.
Manuel M, Iglesias C, Donnet M, Leroy F, Heckman CJ, and Zytnicki D. Fast kinetics, high-frequency oscillations, and subprimary firing range in adult mouse spinal motoneurons. *J Neurosci* 29: 11246-11256, 2009.
Manuel M, and Zytnicki D. Alpha, beta and gamma motoneurons: functional diversity in the motor system's final pathway. *J Integr Neurosci* 10: 243-276, 2011.
Miles GB, Yohn DC, Wichterle H, Jessell TM, Rafuse VF, and Brownstone RM. Functional properties of motoneurons derived from mouse embryonic stem cells. *J Neurosci* 24: 7848-7858, 2004.
Milligan CJ, Edwards IJ, and Deuchars J. HCN1 ion channel immunoreactivity in spinal cord and medulla oblongata. *Brain Res* 1081: 79-91, 2006.
Milner-Brown HS, Stein RB, and Yemm R. Changes in firing rate of human motor units during linearly changing voluntary contractions. *J Physiol* 230: 371-390, 1973.
Monster AW, and Chan H. Isometric force production by motor units of extensor digitorum communis muscle in man. *J Neurophysiol* 40: 1432-1443, 1977.
Mynlieff M, and Beam KG. Developmental expression of voltage-dependent calcium currents in identified mouse motoneurons. *Dev Biol* 152: 407-410, 1992.
Ota F, Connor NP, and Konopacki R. Alterations in contractile properties of tongue muscles in old rats. *Ann Otol Rhinol Laryngol* 114: 799-803, 2005.
Pilarski JQ, Wakefield HE, Fuglevand AJ, Levine RB, and Fregosi RF. Developmental nicotine exposure alters neurotransmission and excitability in hypoglossal motoneurons. *J Neurophysiol* 105: 423-433, 2011.
Powers RK, and Binder MD. Input-output functions of mammalian motoneurons. *Reviews of physiology, biochemistry and pharmacology* 143: 137-263, 2001.

Rank MM, Flynn JR, Battistuzzo CR, Galea MP, Callister R, and Callister RJ. Functional changes in deep dorsal horn interneurons following spinal cord injury are enhanced with different durations of exercise training. *J Physiol* 593: 331-345, 2015.
Rende M, Giambanco I, Buratta M, and Tonali P. Axotomy induces a different modulation of both low-affinity nerve growth factor receptor and choline acetyltransferase between adult rat spinal and brainstem motoneurons. *J Comp Neurol* 363: 249-263, 1995.
Rivera-Arconada I, and Lopez-Garcia JA. Characterisation of rebound depolarisation in mice deep dorsal horn neurons in vitro. *Pflugers Arch* 467: 1985-1996, 2015.
Schwarz EC, Thompson JM, Connor NP, and Behan M. The effects of aging on hypoglossal motoneurons in rats. *Dysphagia* 24: 40-48, 2009.
Stifani N. Motor neurons and the generation of spinal motor neuron diversity. *Front Cell Neurosci* 8: 293, 2014.
Stuart DG, and Brownstone RM. The beginning of intracellular recording in spinal neurons: facts, reflections, and speculations. *Brain Res* 1409: 62-92, 2011.
Tadros MA, Farrell KE, Schofield PR, Brichta AM, Graham BA, Fuglevand AJ, and Callister RJ. Intrinsic and synaptic homeostatic plasticity in motoneurons from mice with glycine receptor mutations. *J Neurophysiol* 111: 1487-1498, 2014.
Tadros MA, Lim R, Hughes DI, Brichta AM, and Callister RJ. Electrical maturation of spinal neurons in the human fetus: comparison of ventral and dorsal horn. *J Neurophysiol* 114: 2661-2671, 2015.
Takahashi T. Inward rectification in neonatal rat spinal motoneurones. *J Physiol* 423: 47-62, 1990a.
Takahashi T. Membrane currents in visually identified motoneurones of neonatal rat spinal cord. *J Physiol (Lond)* 423: 27-46, 1990b.
Umemiya M, and Berger AJ. Properties and function of low- and high-voltage-activated Ca2+ channels in hypoglossal motoneurons. *J Neurosci* 14: 5652-5660, 1994.
Viana F, Bayliss DA, and Berger AJ. Repetitive firing properties of developing rat brainstem motoneurones. *J Physiol (Lond)* 486 (Pt 3): 745-761, 1995.
Vinay L, Brocard F, Pflieger JF, Simeoni-Alias J, and Clarac F. Perinatal development of lumbar motoneurons and their inputs in the rat. *Brain Res Bull* 53: 635-647, 2000.
Wimmer VC, Reid CA, So EY, Berkovic SF, and Petrou S. Axon initial segment dysfunction in epilepsy. *J Physiol* 588: 1829-1840, 2010.
Yarom R, Sagher U, Havivi Y, Peled IJ, and Wexler MR. Myofibers in tongues of Down's syndrome. *J Neurol Sci* 73: 279-287, 1986.
Zagoraiou L, Akay T, Martin JF, Brownstone RM, Jessell TM, and Miles GB. A cluster of cholinergic premotor interneurons modulates mouse locomotor activity. *Neuron* 64: 645-662, 2009.

637 ***Figure Legends***

638

639 ***Figure 1. Comparison of the afterhyperpolarization (AHP) current properties in***
640 ***HMs and SMs.***

641 **A**. Representative recording of the AHP current in a HM in response to a 50 mV
642 voltage step (holding potential -60 mV; 2 ms duration). **B-D**. Bar plots of the
643 amplitude (**B**), time to peak (**C**) and decay time constant (**D**) of HMs (dark grey) and
644 SMs (light grey). Whilst HMs displayed a larger AHP amplitude, no differences were
645 observed for the time to peak and decay time constant.

646

647 ***Figure 2. AP discharge following step injection.***

648 **A**. Representative traces from a single HM during increasing levels of step current
649 injection (1 s duration; lower right panel). **B**. Plots of mean frequency versus current
650 injected for HMs (filled circles) and SMs (open circles). Current injected normalized
651 to rheobase. * indicates d > 0.8; ES large. HMs discharged APs with higher
652 frequencies at rheobase, and the highest intensity current injected.

653

654 ***Figure 3. AP discharge in response to triangular ramp current injection.***

655 **A**. Representative response of a single HM to triangular ramp current injection (0.33
656 nA/s, dashed line). For each MN the current where AP discharge began (on) and
657 ceased (off) was measured. ΔI values were calculated as the difference between these
658 values. **B**. Bar plot of the maximum firing rate measured for HMs (dark grey) and
659 SMs (light grey, * indicates d > 0.8; ES large). **C & D**. Frequency/time (**C**) and
660 frequency/current (**D**) plots for the HM shown in A. All recorded HMs and SMs
661 displayed similar linear increases and decreases of frequency relative to current. **E &**
662 **F**. Frequency histograms for HMs (**E**) and SMs (**F**) where ΔI values have been
663 grouped into 5 pA bins. Solid and hashed bars represent MNs with negative and
664 positive ΔI values, respectively. HMs discharged a greater maximum frequency
665 during ramp current injection compared to SMs, although no differences in ΔI values
666 or distributions were observed.

667

668 ***Figure 4. Responses of MNs to hyperpolarizing current injection.***

669 **A**. Representative recording from a single HM in response to hyperpolarizing current
670 steps (1 second duration) of increasing amplitude. Note the pronounced "sag" that
671 occurs during the hyperpolarizing step (between solid and open triangles). Rebound

depolarization and AP discharge (on some occasions) was observed at the conclusion of the current step. **B**. Bar plot showing the sag ratio of HMs (dark grey) and SMs (light grey). Sag ratio was calculated by comparing the membrane potential at the onset (solid triangle) and offset (open triangle) of the hyperpolarizing step. Sag ratios did not differ between HMs and SMs. **C**. Bar plot illustrating the proportion of HMs (dark grey) and SMs (light grey) exhibiting AP discharge at conclusion of current step (as shown in A). The remaining MNs in both populations only displayed rebound depolarization without AP discharge.

Figure 5. Excitatory synaptic drive in HMs and SMs.

A. Trace showing representative spontaneous excitatory postsynaptic currents (sEPSCs, 30 s of continuous data) in a HM. **B**. Representative sEPSC extracted and averaged from trace in A. **C-F**. Bar plots comparing the frequency (**C**), amplitude (**D**), rise time (**E**) and decay time constant (**F**) for HMs (dark grey) and SMs (light grey). These data demonstrate that excitatory drive differs between HMs and SMs.

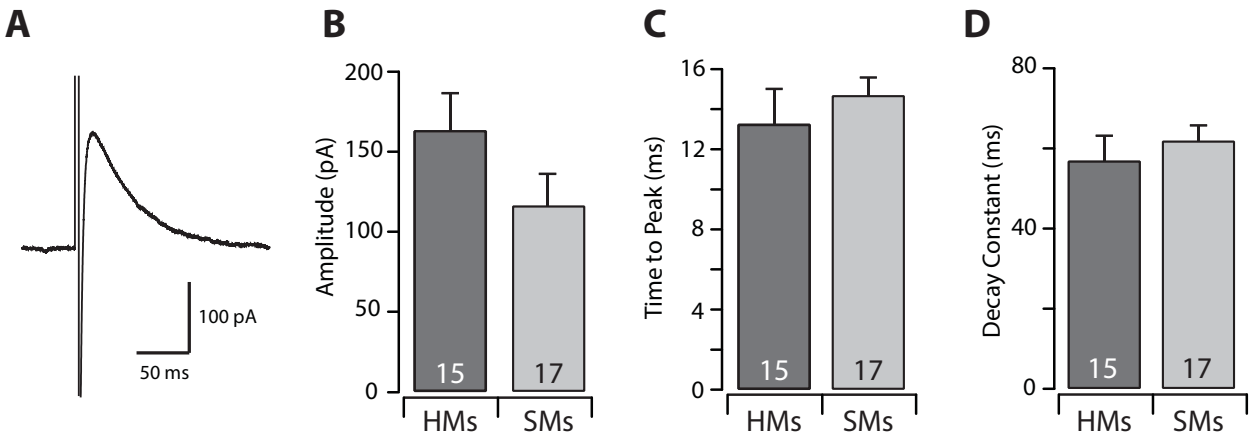

Figure 1
Tadros et al

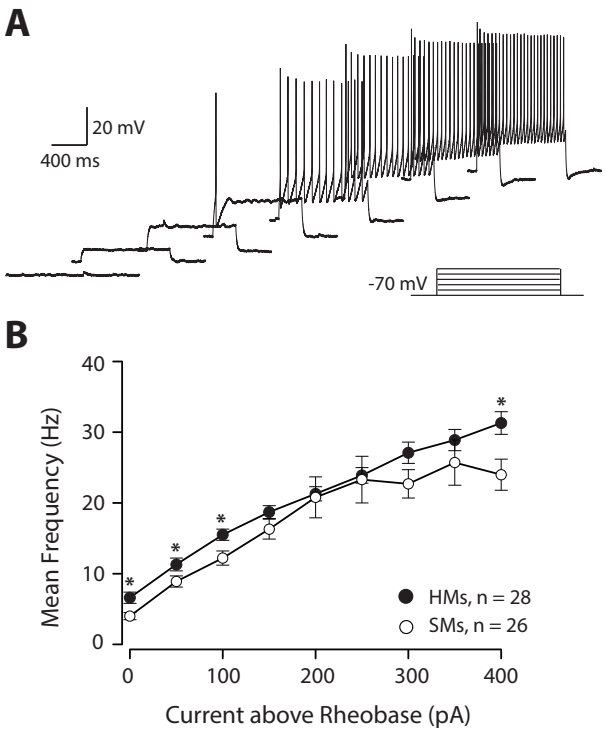

Figure 2
Tadros et al

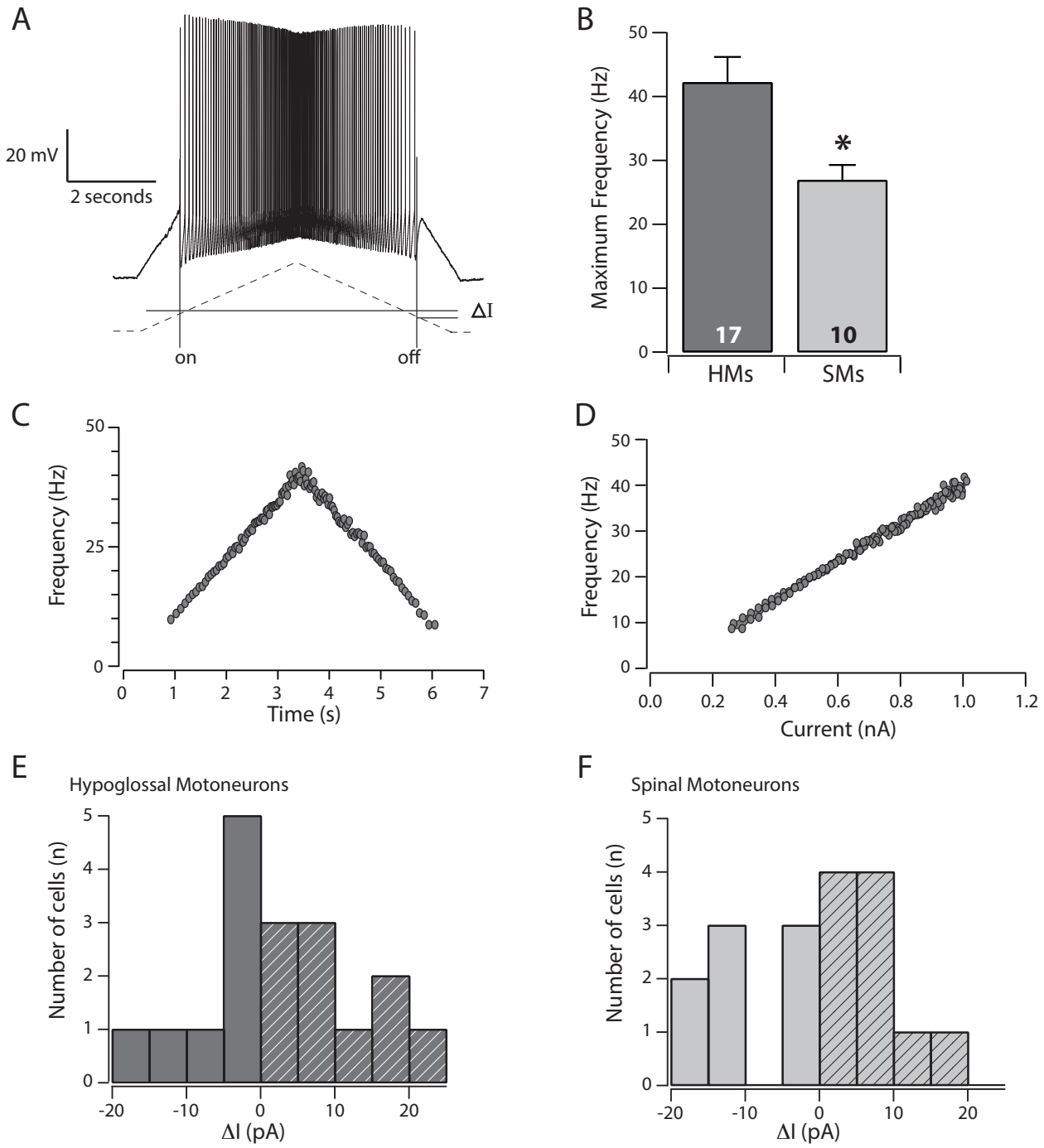

Figure 3
Tadros et al

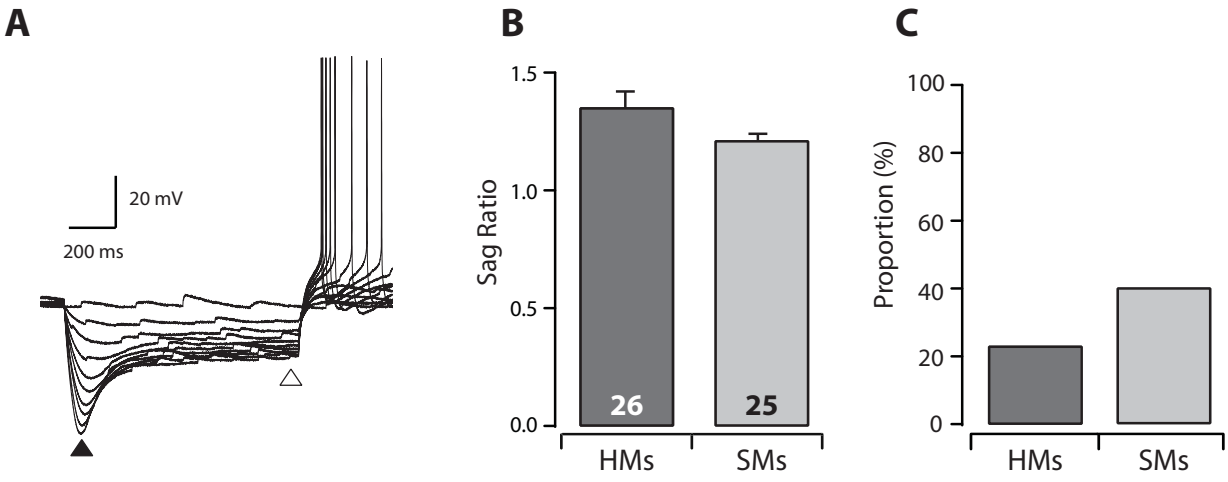

Figure 4
Tadros et al

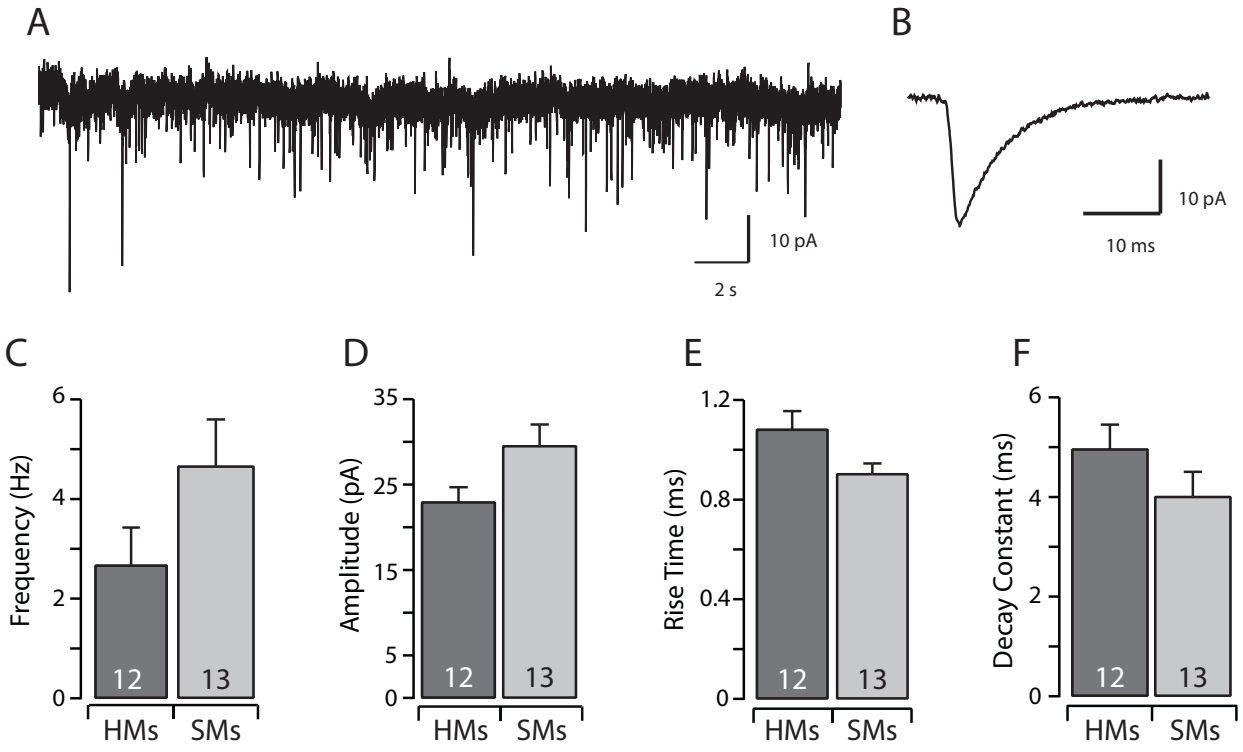

Figure 5
Tadros et al

Table 1. Intrinsic properties of HMs and SMs

	Hypoglossal (HMs)	**Spinal (SMs)**	**Effect Size (Cohen's d)**
Animal Age (days)	8.9 ± 0.8	8.4 ± 0.3	
Number of cells	28	26	
Input Resistance (MΩ)	97 ± 10	147 ± 21	Moderate (d = 0.60)
RMP (mV)	-69.8 ± 0.9	-66.0 ± 1.7	Moderate (d = 0.55)
Rheobase (pA)	489 ± 63	346 ± 49	Moderate (d = 0.54)
AP Threshold (mV)	-53.3 ± 1.0	-55.6 ± 1.6	Small (d = 0.39)
AP Amplitude (mV)	68.9 ± 2.0	69.3 ± 3.4	Trivial (d = 0.03)
AP Rise Time (ms)	0.46 ± 0.03	0.65 ± 0.04	Large (d = 1.19)
AP Peak velocity (dV/dT; mV/ms)	168.7 ± 11	133.2 ± 12	Large (d = 0.87)
AP Peak voltage acceleration (d^2V/dT^2; mV/ms^2)	0.43 ± 0.05	0.19 ± 0.02	Large (d = 1.41)
AP Half-width (ms)	0.95 ± 0.03	1.49 ± 0.08	Large (d = 1.98)
AHP Amplitude (mV)	-24.3 ± 1.0	-20.5 ± 1.9	Moderate (d = 0.57)
F/I Rheobase (pA)	288 ± 43	210 ± 40	Small (d = 0.36)
F/I minimum rate (Hz)	6.20 ± 0.76	3.87 ± 0.53	Moderate (d = 0.68)
F/I gain (Hz/pA)	0.068 ± 0.004	0.075 ± 0.008	Small (d = 0.20)
Sag Ratio	1.35 ± 0.07	1.21 ± 0.03	Small (d = 0.47)
Rebound Spiking (%)	23	40	
ΔI (pA)	+2.51 ± 2.4	-0.60 ± 2.4	Small (d = 0.30)
Maximum firing rate (Hz)	42.2 ± 4.0	26.9 ± 2.4	Large (d = 1.19)
Ramp gain (Hz/pA)	48.3 ± 4.1	32.9 ± 2.8	Large (d = 1.14)

AP properties (rows 5-12) are based on APs generated in response to 2 ms step, F/I properties (rows 13-15) are based on repetitive discharge elicited during 1 second current step injection. F/I gain was calculated across the first 6 successive current intensities. All values presented as mean ± SEM.